Characterization and performance of co-axial HPGe detectors

Sanjeet S. Kaintura[1] · Swati Thakur[1] · Soni Devi[1] · Katyayni Tiwari[1] · Priyanka Raizada[1] · Amanjot[1] ·
Subham Kumar[1] · Pushpendra P. Singh[1,2]

Abstract
High purity germanium (HPGe) detectors are deployed globally for gamma-radiation spectroscopy due to their superior energy resolution. In this work, the essential characteristics of n and p-type HPGe detectors, such as energy resolution, efficiency, minimum detectable activity (MDA), and peak shape were studied for the purpose of characterization and performance optimization. The results are obtained for various source-detector configurations in a wide energy range of 40–1408 keV using gamma sources, such as ^{109}Cd, ^{57}Co, ^{137}Cs, ^{54}Mn, ^{65}Zn, ^{60}Co, and ^{152}Eu. Scanning (distance, lateral, and radial) of the detectors was performed using different gamma sources to understand the orientation of the crystal with its active volume and counting efficiency and to characterize the geometry in detail. The ambient background around the n-type HPGe was reduced using Pb-shielding. As a result, an 85.85% suppression was observed in the mean integral window of 40–2700 keV. The characterization and performance tests of the detectors convincingly suggest that both the detectors can be deployed for environmental radioactivity explorations.

Introduction

HPGe detectors set the gold standard in the domain of gamma-ray spectroscopy due to their exceptionally good energy resolution. As a result, the HPGe detectors are preferred over NaI(Tl) detectors for addressing unresolved gamma spectral lines in complex scenarios [1, 2]. Gamma-ray spectrometry using HPGe is an excellent solution for nondestructive technique and hence applied for the identification and quantification of enigmatic radionuclides (natural as well as artificial) [3, 4].

To investigate the radiopurity in a specific measuring geometry, accurate knowledge about detection efficiency over a wider energy range is crucial [5]. The different factors that affect the detector efficiency include detector volume, source geometry, source-detector distance, crystal size and type, cross-section, and dead layer of the detector [6]. An increase in the dead layer leads to a decrease in efficiency not only due to gamma attenuation in the dead layer but also due to the reduced active volume of the detector [7]. For measuring low radioactive environmental samples, a source close to the detector geometry (e.g., a Marinelli beaker shape that fits in the detector and cylindrical shape) is often preferred to achieve high counting efficiency [8].

Other essential parameters that significantly affect the performance of detectors are MDA, peak shapes, such as full width at half maxima (FWHM), full width at tenth maxima (FWTM), full width at fiftieth maxima (FWFM), and Peak-to-Compton (P/C) ratio, etc. The MDA is defined as the lowest amount of radioactivity present in a source or sample that can be measured by a detection system. The concept of MDA plays a crucial role in radionuclide quantification at low levels, which reflects the capability of the gamma spectrometer in terms of its detection limit [9, 10]. The peak shape of spectral lines by carrier information is used to achieve peak shape discrimination (PSD). FWHM imparts knowledge about the resolution of the detector and the worsening of the tail of the peak can be estimated by

✉ Sanjeet S. Kaintura
  sanjeet.19phz0010@iitrpr.ac.in

1 Department of Physics, Indian Institute of Technology Ropar, Rupnagar, Punjab 140001, India

2 iHub – AWaDH, Indian Institute of Technology Ropar, Rupnagar, Punjab 140001, India

FWTM and FWFM. The P/C ratio is similar to signal-to-noise ratio and hence low P/C ratio reflects poor energy resolution [11, 12].

To assess the radioactivity level in a sample using the HPGe detector, it is inevitable to measure the environmental background radioactivity a priori. In the Earth's environmental background, ~80% of the contribution is due to natural radioactivity, in which primordial radionuclides, such as ^{238}U, ^{232}Th, their decay chain products, and ^{40}K radionuclides are the major contributors. On the other hand, radiations due to artificial interferences, such as nuclear fallout at specific locations can not be ignored [13–18]. These radionuclides spontaneously disintegrate to achieve stability by emitting α, β, and γ-rays, γ-rays being the most penetrating radiations of them all [17]. The exposure (external and internal) of these harmful radiations to living beings depends on the abundance of naturally occurring gamma-emitting radionuclides present in the soil and rock [17], therefore, research on radionuclides in soil and rock has been explored in the last ten to twenty years worldwide [19]. It has been found that ^{238}U, ^{232}Th, and ^{40}K (having $T_{1/2} \sim 10^9$–10^{10} years) contribute 25, 40, and 35% of the absorbed gamma dose rate in the outer environment received by the public globally [20, 21]. In order to use the HPGe detectors, registered background data facilitates the experimentalist to extrapolate the detector performance from data quoted by the manufacturer to ensure its optimum operating condition in comparison to the claimed range [22]. However, low-level radioactivity other than the sample can be contributed substantially (several tens of percent) by the background during the measurement which can fluctuate the counting statistics of the sample and reduce the reliability of the measurement setup [13]. Therefore, to remove the contributions other than the low-level radioactive sample, it is necessary to reduce the ambient background, and this requires careful selection of shielding materials. The fact that Lead (Pb) offers the best sensitivity among all preferred materials is highly dense (11,340 kg m^{-3}) with a high atomic number (Z = 82), resulting in the effective suppression of background [23].

For highly sensitive gamma-ray spectroscopy, performance evaluation of the HPGe detector is essential. With this motivation, we have characterized two coaxial HPGe detectors of opposite polarity (one is p-type and the other is n-type). These detectors will be deployed to investigate radioactivity in the ambient background in the lab and various representative soil, rock, and vegetation samples collected from different locations in a particular geographic region. This radioactivity concentration from samples will be helpful to determine the radiation dose, and hazard level, and reveal the radiological impact on the public residing in the area. There may be some variation in the performance of both the detectors due to various physical parameters. Hence, optimization of various performing parameters as

well as the working conditions of these spectrometers would be helpful prior to their further use for actual radioactivity measurement. Therefore, our objective in the present work is threefold:

(1) Standard characterization and performance evaluation of n and p-type HPGe detectors based on different parameters using various standard gamma-ray sources.

(2) Detailed characterization of both detectors by scanning (distance, lateral, and radial) of the crystals and spectral analysis.

(3) Intercomparison between the performance of n and p-type HPGe detectors on the basis of efficiency and background spectral analysis.

Experimental details

For the characterization and performance evaluation of the detectors, the detectors were cooled with liquid nitrogen (LN$_2$) and biased at the optimum voltage as provided by the manufacturer. The p-type HPGe (CANBERRA GC2018-10862) detector was biased at + 2500 V while the n-type HPGe (ORTEC GMX-20-70-S) was biased at − 3000 V. The signals generated after biasing were subsequently subjected to amplification and pulse-shaping processes, and recorded with NIM based data acquisition system (DAQ) consisting of an 8 K multi-channel analyzer (MCA). MAESTRO software was used to collect and readout the data. The collected data were analyzed offline using linux advanced multi parameter system (LAMPS) analysis software [24]. The n-type detector, p-type detector, and schematic of the whole experimental setup in shielded configuration have been showcased in Fig. 1a–c, respectively. The specifications of the detectors for the experimental configuration have been documented in Table 1. The detectors were subjected to characterization over an energy range 39.52–1408.01 keV, utilizing various point-type gamma sources, such as ^{109}Cd, ^{57}Co, ^{137}Cs, ^{54}Mn, ^{65}Zn, ^{60}Co, and ^{152}Eu, etc. The data were collected using standard gamma sources for more than 10,000 counts for better statistics. The details of standard sources used in the present work with their gamma-ray energies are given in Table 2.

Both the detectors were characterized on the basis of absolute efficiency to understand the crystal geometry, active volume, and exact position of the crystal by irradiating with different gamma sources. The distance scan (D$_s$) of detectors was conducted along their cylindrical axis at a distance of 5 to 30 cm from the top face with an interval of 5 cm at low (88.0 keV), middle (661.7 keV) and high energy (1332.5 keV). Radial scanning (R$_s$) was performed parallel to the detector diameter from − 65 to + 65 mm concerning the crystal center (R$_s$ = 0) and lateral scanning (L$_s$) was done

Fig. 1 **a** Be window-based n-type HPGe. **b** Al window-based p-type HPGe detector. **c** A schematic of the whole experimental setup in the shielded configuration. **d** Schematic of HPGe detectors showing the detector assembly with directional indicators during scanning. L and d are length and diameter of the crystal

Table 1 Detector specification of both p-type and n-type HPGe detectors

Specification	p-type (GC-2018)	n-type (GMX-20)
Geometry	Closed end	Closed end
Crystal diameter	61.80 mm	53.00 mm
Crystal length	31.00 mm	49.50 mm
Core hole diameter	7.50 mm	8.70 mm
Core hole depth	16.00 mm	41.50 mm
Net volume of the crystal	92.28 mm^3	106.74 mm^3
Window (thickness)	Al (1.6 mm)	Be (0.5 mm)
Crystal distance from window	4.78 mm	3.00 mm

along the detector length from -20 to $+40$ mm with reference to the detector face ($L_s = 0$) as shown in Fig. 1d. Radial and lateral scanning were performed with the step size of 5 mm while the source-detector distance was maintained at

10 mm throughout the scanning. The gamma sources utilized for scanning have an active diameter of ~6 mm and a thickness of ~1 mm. In close geometry scanning (radial and lateral), only 1115.5 keV was used instead of 1332.5 keV to avoid coincidence summing during the counting. Scanning was performed without a collimator using standard gamma sources. The manual placement uncertainty in position is found to be ≤ 1 mm. A similar scanning methodology for modeling a carbon fiber loaded HPGe detector has been used and may be found in ref. [25]. The ambient background was acquired using both the detectors and compared for better understanding of the environmental radioactivity. In order to reduce the environmental radioactivity, preceding the LN$_2$ dewar, the HPGe detector is enveloped by a discrete passive shielding system composed of lead bricks measuring 22.9 cm $\times$ 7.6 cm $\times$ 5.1 cm. The background obtained in the n-type HPGe detector with and without Pb-shielding was

Table 2 Details of gamma lines emitted from their respective sources during experiment

Radioactive source	Energy in keV (intensity in %)	Half life (days)
^{109}Cd	88.0(3.64)	461.4
^{57}Co	122.1(85.6), 136.5(10.68)	271.7
^{137}Cs	661.7(85.1)	10,986.5
^{54}Mn	834.9(50.04)	312.2
^{65}Zn	1115.5(99.97)	243.9
^{60}Co	1173.2(99.85), 1332.5(99.98)	1923.6
^{152}Eu	39.5(21.00), 121.8(28.53), 244.7(7.55), 344.3(26.59), 411.1 (2.24), 444.0(2.83), 778.9(12.93), 867.4(4.23), 964.1(14.51), 1085.8(10.11), 1089.7(1.73), 1112.1(13.67), 1213.0(1.42), 1299.1(1.63), 1408.0(20.87)	4933.7

compared with each other and the measured soil level was analyzed.

Quantifying parameters

Different parameters were evaluated for the characterization and performance of n and p-type HPGe detectors. These essential parameters are peak shape, P/C ratio, resolution, efficiency, MDA, and figure of merit (FoM), etc.

Full width at half maxima

Full width at half maxima (FWHM) is a significant parameter to estimate the peak shape which tells the separation between two closely spaced energies [11, 26, 27]. FWHM was evaluated manually using the following equation [12]:

$$FWHM = \frac{\Delta E}{C_2 - C_1 + 1} \times N_r \qquad (1)$$

Here, ΔE is the energy difference between 1332.5 keV and 1173.2 keV, and is also known as the conversion factor. C_2 and C_1 are peak channels at 1332.5 keV and 1173.2 keV, respectively. The unity factor 1 in this equation is the uncertainty in channel number, and N_r is the width of the reference peak (i.e., FWHM, FWTM, and FWFM) in terms of channel numbers. It is calculated by taking the difference between the channel numbers on the right side and the left side for specific peak shapes of interest, namely, FWHM, FWTM, and FWFM. The channel numbers were determined using specific formulas: (C-B)/2 for FWHM, (C-B)/10 for FWTM, and (C-B)/50 for FWFM. Here, C represents peak counts and B is the background counts. The channel number points on both the left and right sides have been distinctly marked with arrows in the typical peak shape in Fig. 2. This figure also

Fig. 2 Typical peak shape indicating FWHM, FWTM and FWFM in a photo-peak [11]
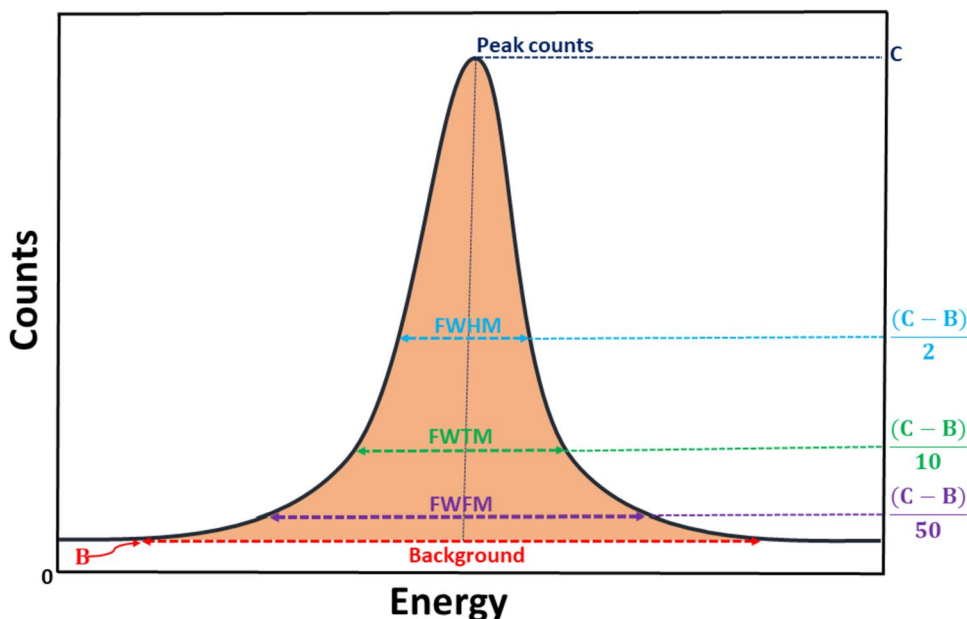
illustrates the typical peak shape of a gamma line, including FWHM, FWTM, and FWFM, all derived from their respective net counts. Also, FWTM and FWFM are analogically calculated as FWHM described in above Eq. (1).

Peak-to-Compton ratio

Peak-to-Compton ratio (P/C) is an essential parameter to have an idea about the quality of signals and it can be calculated as follows [11, 28]:

$$\frac{P}{C} = \frac{\text{Total peak counts at 1332.5 keV}}{\text{Average counts per channel between 1040 keV to 1096 keV}} \tag{2}$$

Hence, it can be concluded that the higher P/C ratio will lead to better energy resolution and vice-versa.

Minimum detectable activity

Minimum detectable activity (MDA) is one of the significant parameters to check the sensitivity of the detector and it can be calculated by the most widely used Curie's equation [29] which is given as:

$$MDA = \frac{2.706 + 4.653\sqrt{C_B}}{P \times \mathcal{E} \times t} \tag{3}$$

where C_B is the background counts, P is the transition probability or intensity of specific gamma photon, ε is the absolute efficiency of the detector at the same energy and t is counting time.

Efficiency

To measure the signals in the detector, the absolute efficiency (ε) of the detector plays an extremely important role. It shows the total counts per unit time (cps) to the detector relative to the total present activity (A) of the source at a particular energy [28, 30, 31] i.e.,

$$\varepsilon = \frac{cps}{A \times P} \times 100\% \tag{4}$$

P is the transition probability, sometimes called the intensity of gamma photon at a particular energy (E).

Relative efficiency (η) is the absolute efficiency of the HPGe detector relative to the efficiency (1.2×10^{-3}) of $3'' \times 3''$ NaI(Tl) scintillation detector using a ^{60}Co gamma source at 1332.5 keV energy when source-detector distance is 25 cm [28].

Figure of merit

The choice of detector depends upon the figure of merit (FoM), which is given by [28]:

$$FoM = \eta \times \sqrt{\left(\frac{\frac{P}{C}}{FWHM}\right)} \tag{5}$$
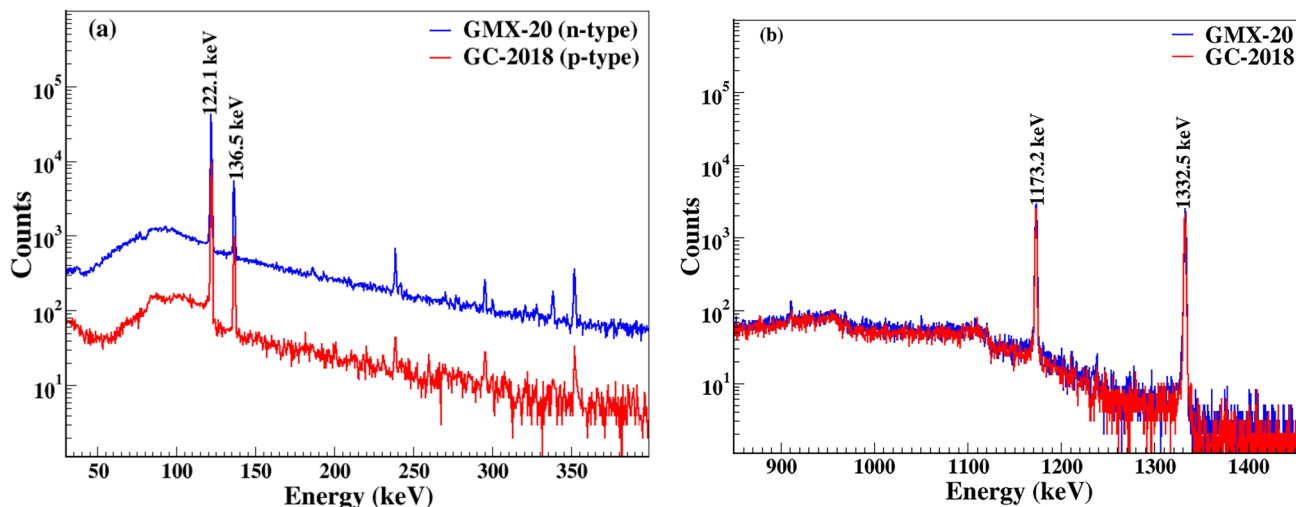

Fig. 3 **a** Spectra of ^{57}Co using both detectors **b** spectra of ^{60}Co using both detectors

Analysis

At the initial stage, the significant properties and various performance checks of the detectors were carried out. The analyzed resolution of the p-type detector in terms of FWHM is (0.83 ± 0.01) keV while that for n-type HPGe is (0.84 ± 0.01) keV corresponding to 122.1 keV of ^{57}Co at source-detector distance of 25 cm. Both, p and n-type detectors have relative efficiency of 24.61 and 25.56%, and FWHM (1.92 ± 0.02) keV and (1.87 ± 0.02) keV respectively, at 1332.5 keV irradiated energy from ^{60}Co gamma source. The obtained spectra of ^{57}Co and ^{60}Co are shown in Fig. 3a, b.

Energy calibration was performed to convert the channel numbers into the energy scale and the variation of FWHM with energy was analyzed. The relationship between the channel numbers and FWHM with energy in both detectors using ^{152}Eu and ^{137}Cs gamma sources at 25 cm has

been carried out and shown in Fig. 4a, b. In Fig. 4a, the lines connecting data points represent regression functions, $y_n = a_n x + b_n$ (where, n = 1 corresponds to p-type, and n = 2 for n-type HPGe). The precision-derived parameters for p-type are $a_1 = (0.47131 \pm 1.54437 \times 10^{-5})$ and $b_1 = (0.40792 \pm 0.0284)$, while for n-type HPGe, they are $a_2 = (0.41215 \pm 1.4304 \times 10^{-5})$ and $b_2 = (0.64554 \pm 0.03008)$. Two distinct slopes correspond to two distinct gains. Each data point recorded by the detector has an ideal statistical correlation coefficient of 1. In Fig. 4b, increasing the FWHM with energy also has a strong correlation (r = 0.99) with the strong coefficient of determination ($R^2 = 0.998$ for p-type and $R^2 = 0.995$ for n-type HPGe) signifying the continuous variation of the signal fluctuations in an equal order. Efficiency was calibrated using the activities of sources for their respective gamma lines for a particular distance.
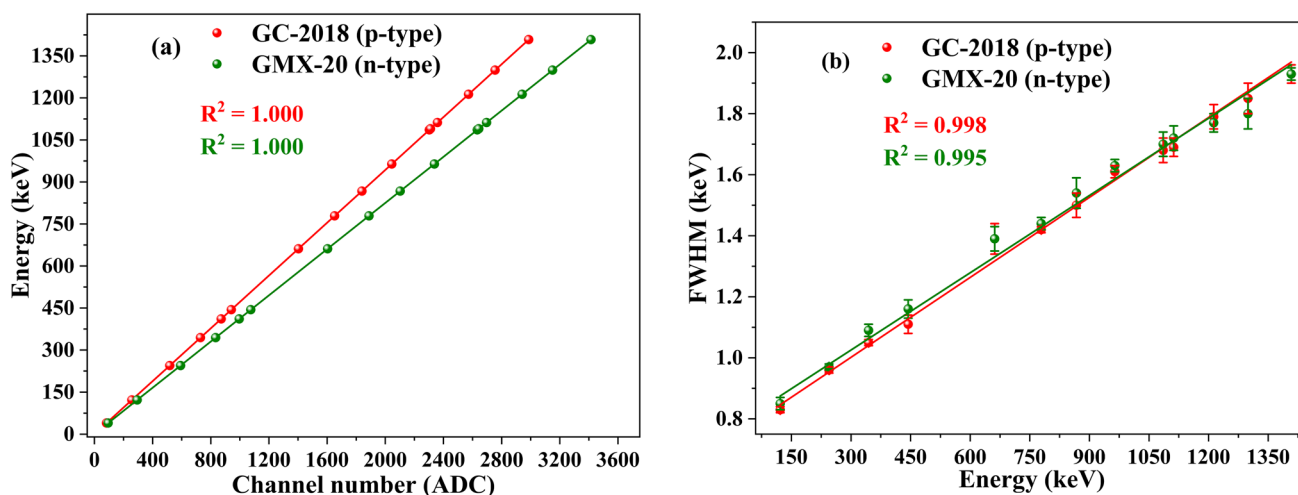

Fig. 4 **a** Variation of energy with channel number in both testing detectors using different gamma sources **b** variation of FWHM with energy in both testing detectors using different gamma sources

Table 3 Evaluation and comparison of different parameters in both detectors

Specification	GC-2018 (p-type)			GMX-20 (n-type)			Acceptable values [11, 28]
	S	F	M	S	F	M	
FWHM @ 122.1 keV	0.85	0.81 ± 0.11	0.85	0.81	0.80 ± 0.09	*	0.8 to 2.4
FWHM @ 1332.5 keV	1.88	1.90 ± 0.18	1.64	1.84	1.85 ± 0.16	1.79	1.7–2.7 for n-type & 1.7–2.5 for p-type
FWTM/FWHM @ 1332.5 keV	1.85	1.73 ± 0.23	1.85	1.89	1.89 ± 0.21	1.90	≤ 1.9
FWFM/FWHM @ 1332.5 keV	2.75	2.84 ± 0.32	*	2.49	2.56 ± 0.26	2.70	2.5 for n-type & ≤ 2.8 for p-type
η @ 1332.5 keV (%)	*	24.61 ± 1.43	23.90	*	25.56 ± 1.54	23.00	Not specified
P/C Ratio @ 1332.5 keV	*	$(49.3 \pm 7.0):1$	56.7:1	*	$(45.2 \pm 5):1$	52:1	40:1–110:1
FoM @ 1332.5 keV	*	1.26 ± 0.22	*	*	1.26 ± 0.18	*	Not specified

S = Measured by software, F = Determined by formula, M = Provided by manufacturer

*The values are neither quoted by the manufacturer nor displayed by the software

Results and discussion

Performance parameters

The various essential parameters for both HPGe detectors compared with software measurements (S), determined manually using formulae (F) as mentioned in Eqs. (1), (2), (4), (5) and analogous to Eq. (1), and specified by manufacturer (M) are given in Table 3. These values are further compared with nominal values provided in the literature [11, 28]. All the values are similar and close to the values quoted by the manufacturer, as well as the nominal range values reported in the literature. The cumulative count rate recorded to measure the FWHM and P/C ratio in the p-type HPGe detector was 10.06 counts per second having 34.1 kBq source activity, while in the n-type HPGe detector, 9.56 counts per second were registered using 31.2 kBq source activity at an energy of 1332.5 keV when positioned at a 25 cm source-detector distance. The variation of absolute efficiency with
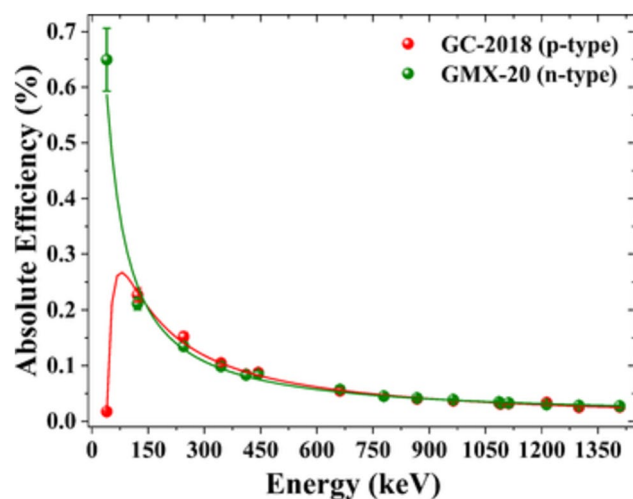
Fig. 5 Variation of absolute efficiency with energy in both testing detectors employing gamma sources at 25 cm

energy using gamma sources (^{152}Eu, and ^{137}Cs) at a sources-detector distance of 25 cm is represented in Fig. 5. It shows that no significant change was observed in the efficiency curve of both detectors, except 39.5 keV which is the lowest measured energy to quantify the efficiency. The reason is that thin layers of contacts of semiconducting materials are fabricated in a detector to swipe the charge carriers for a signal response. This fabrication in a detector is made in such a way that it has a thick (~ 600 μm) n$^+$ contact usually made up of lithium donor and a thin (~ 0.3 μm) p$^+$ contact of boron receptor. If the contacts are configured in such a way that the n$^+$ is outer contact on the layer of the detector and p$^+$ is inner contact then on passing the gamma photon through this, there is negligible attenuation with the high energetic gamma photon like 661.7 keV but, drastic transmission loss is appeared at low energy photon as 46.5 keV. It has a direct impact on the efficiency of the detector for the same energy region. Such a detector is known as the 'p' type. On the other hand, if the configuration of contacts is reversed and thin p$^+$ is an outer contact while thick n$^+$ is an inner contact then there is no attenuation in the low energy region, and suitable to analyze the low energy photon. This detector is called the 'n' type [22]. It is crucial to emphasize that the enhanced efficiency of n-type HPGe at lower energy is also due to a thin beryllium (Be) window, whereas a thick aluminium (Al) window is utilized in p-type HPGe.

To determine the limit of detection in both gamma spectrometers, the MDA was assessed at source-detector distances of 5, 10, 15, and 20 cm, as detailed in Table 4. With increasing energy, the MDA should be inversely proportional to the efficiency shown in Fig. 5. However, several other factors can impact the MDA significantly such as the background and intensity (P) of a particular gamma line. At energies below 100 keV, specifically at 88.0 keV, it was expected that there would be a significant difference in the MDA between the p-type and n-type detectors. However, the results presented indicate that while the MDA is indeed higher for the p-type detector, the difference is relatively small. This is due to the presence of background X-rays

Table 4 MDA (in Bq) determined in p-type HPGe and in n-type HPGe using various gamma sources at different distances

Gamma source	Energy (keV)	MDA @ 5 cm		MDA @ 10 cm		MDA @ 15 cm		MDA @ 20 cm	
		p-type	n-type	p-type	n-type	p-type	n-type	p-type	n-type
^{109}Cd	88.0	4.47 ± 0.28	3.85 ± 0.23	9.85 ± 0.63	9.43 ± 0.54	17.49 ± 1.02	15.72 ± 0.90	24.83 ± 1.37	22.87 ± 1.32
^{57}Co	122.1	0.14 ± 0.01	0.17 ± 0.01	0.32 ± 0.02	0.40 ± 0.02	0.58 ± 0.03	0.70 ± 0.04	0.81 ± 0.04	0.99 ± 0.05
^{57}Co	136.5	1.03 ± 0.06	1.39 ± 0.09	2.39 ± 0.14	2.99 ± 0.24	4.12 ± 0.23	5.54 ± 0.45	5.86 ± 0.32	7.59 ± 0.54
^{137}Cs	661.7	0.18 ± 0.02	0.20 ± 0.02	0.41 ± 0.05	0.36 ± 0.04	0.76 ± 0.08	0.59 ± 0.06	1.05 ± 0.11	0.88 ± 0.09
^{54}Mn	834.9	0.19 ± 0.02	0.18 ± 0.02	0.41 ± 0.03	0.39 ± 0.03	0.52 ± 0.04	0.63 ± 0.04	0.84 ± 0.06	0.81 ± 0.05
^{65}Zn	1115.5	0.26 ± 0.04	0.50 ± 0.05	0.77 ± 0.07	1.08 ± 0.09	1.24 ± 0.11	1.56 ± 0.12	1.68 ± 0.14	2.41 ± 0.16
^{60}Co	1173.2	0.18 ± 0.03	0.21 ± 0.03	0.36 ± 0.04	0.40 ± 0.05	0.55 ± 0.07	0.66 ± 0.07	0.87 ± 0.10	1.01 ± 0.11
^{60}Co	1332.5	0.13 ± 0.02	0.18 ± 0.03	0.35 ± 0.05	0.39 ± 0.05	0.62 ± 0.08	0.53 ± 0.07	0.84 ± 0.10	0.81 ± 0.09

emitting the energy at 87.35 keV, originating from [212]Pb and ^{210}Pb radionuclides with intensities of 3.81 and 1.98%, respectively. The 87.35 keV X-rays and 88.0 keV gamma-rays are closely positioned, creating a challenge in distinguishing them due to the limited resolution. Consequently, they overlap, and their collective counts are aggregated to determine the overall background contribution. This factor is dominating over efficiency factor and ultimately impacting the MDA. The calculated MDA for p and n-type detectors was found 4.47 Bq and 3.85 Bq at the energy of 88.0 keV having the source-detector distance of 5 cm but at 20 cm it was found 24.83 Bq and 22.87 Bq, respectively. Furthermore, at 122.06 keV, the intensity becomes pivotal. For instance, if we have 122.06 and 121.78 keV gamma lines originating from [57]Co and [152]Eu, respectively, it is worth noting that these two energies are very close to each other. The proximity of the 122.06 and 121.78 keV gamma lines results in nearly identical efficiencies, falling within the error margin. However, their divergent intensities (85.60% at 122.06 keV and 28.53% at 121.78 keV) significantly influence the overall MDA. Again, ^{137}Cs background radiation, stemming from nuclear fallout and weapon testing with a gamma line at 661.7 keV, leads to slightly higher MDA than 1332.5 keV. The evaluated MDA at 661.7 keV is found to be 0.18 and 0.20 Bq at 5 cm while it is found to be 1.05 and 0.88 Bq at 20 cm in p and n-type HPGe detectors, respectively. The MDA was calculated up to 1332.5 keV and at 1332.5 keV it was found 0.13 and 0.18 Bq at 5 cm while it was 0.84 and 0.81 Bq in p-type and n-type HPGe detectors, respectively at 20 cm. The overall behavior of MDA in both detectors is more or less the same due to the effect

of background counts and transition probability that impact MDA. Additionally, the ratio of MDA values between n-type and p-type detectors has been determined at different distances with various energies and is showcased in Fig. 6. The MDA ratios were evaluated to be 0.53 at a distance of 5 cm and 1.28 at a distance of 15 cm, representing 1115.5 keV and 661.7 keV, respectively. Variations in the MDA ratio are the result of both efficiency and deviations in background counts.

Scanning of n-type and p-type detectors

The distance scan was performed at 88.0 keV (low), 661.7 keV (middle), and 1332.5 keV (high energy) in both the detectors and shown in Fig. 7a–c, respectively. In the distance scan, the highest difference in the efficiencies of both the detectors was observed at 88.0 keV with a relative change of 25.56% when the source-to-detector distance was 5 cm. In the case of middle energy (661.7 keV), both detectors exhibited the maximum absolute efficiency, with a relative change of 5.95%. At the high energy (1332.5 keV), the relative change in efficiency at 5 cm is 2.14% which is minor. It is clear from all the figures that there is a negligible variation in the efficiency from 20 to 30 cm.

The radial scans at 88.0, 661.7, and 1115.5 keV in both detectors are presented in Fig. 8a–c, respectively. The maximum radial efficiency and disparity between p-type and n-type detectors were observed at an energy of 88.0 keV, specifically at a distance of 0 mm (face center of the detector). This suggests that at 0 mm the irradiated gamma-rays encounter more number of gamma photons within the

Fig. 6 MDA ratio computed in p-type to n-type HPGe using various gamma sources at different distances
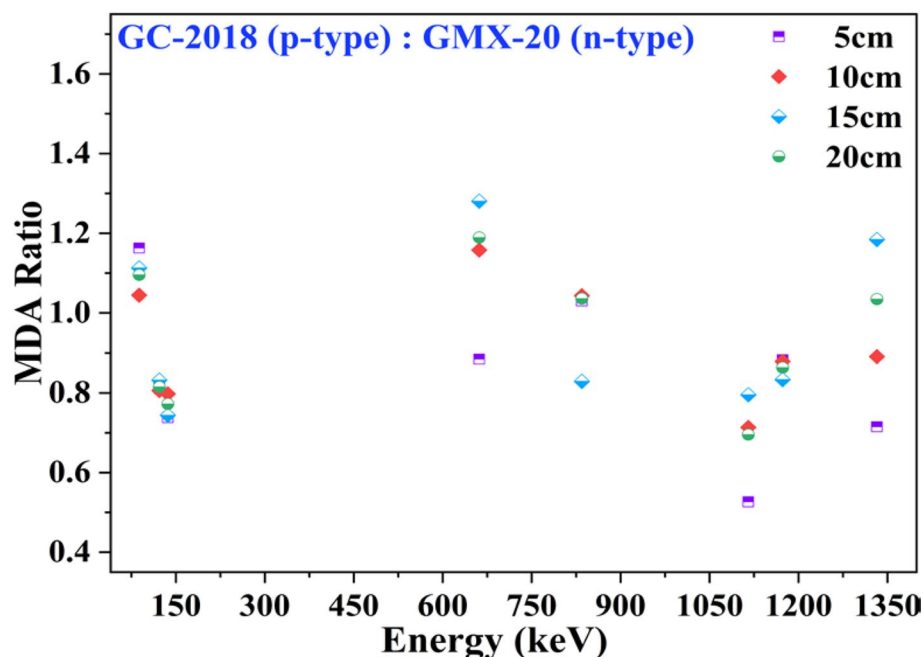
active volume of the crystal in both detectors. The evaluated efficiency at 88.0 keV in both detectors was found with a relative difference of 32.36%. At 661.7 keV, the highest efficiency was observed in p and n-type detectors at 0 and 5 mm, respectively, with a relative difference of 7.49%. At higher energy (1115.5 keV) efficiency with maximum value was found at 0 mm in both detectors having a relative change

of 14.88%. The higher efficiency of p-type GC-2018 is due to its higher radial cross-section which will provide a higher solid angle and hence higher efficiency than n-type HPGe along radial direction.

Last, the lateral scans at 88.0, 661.7, and 1115.5 keV in both the detectors are presented in Fig. 9a–c, respectively. The efficiency along the lateral sides of the detectors was
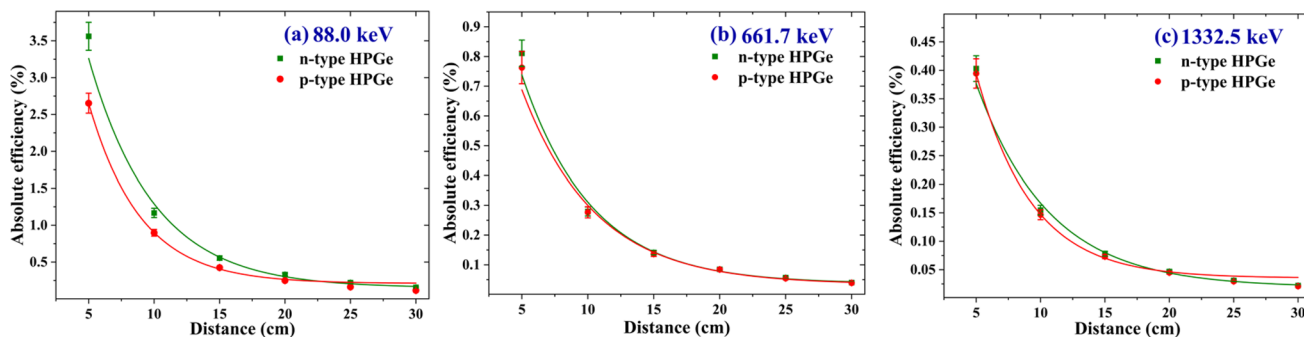
Fig. 7 Absolute photopeak efficiency at the energies of **a** 88.0 keV, **b** 661.7 keV, and **c** 1332.5 keV, plotted against distance scan within the uncertainty of source placement ≤ 1 mm. Solid lines are showing the fitting of the experimental values using fitting function of type, $y = y_0 + A \exp(R_0 x)$, where A and R_0 are constants
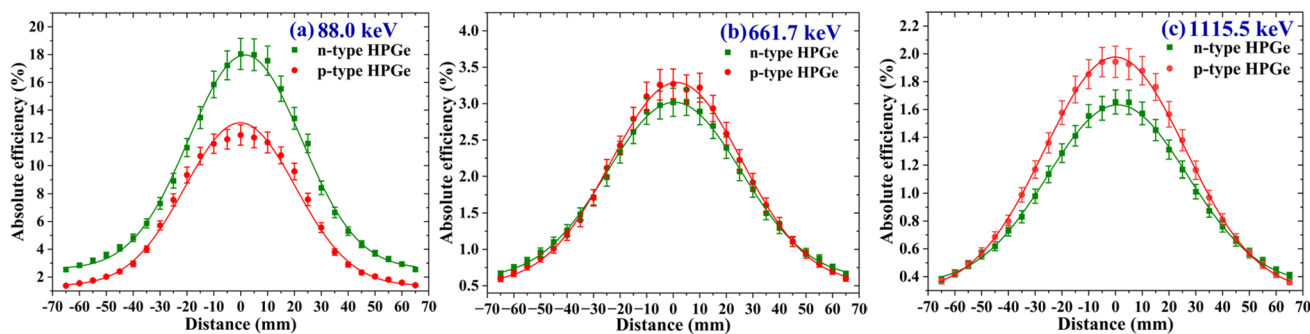
Fig. 8 Absolute photopeak efficiency at the energies of **a** 88.0 keV, **b** 661.7 keV and **c** 1115.5 keV, plotted against radial scan within the uncertainty of source placement ≤ 1 mm
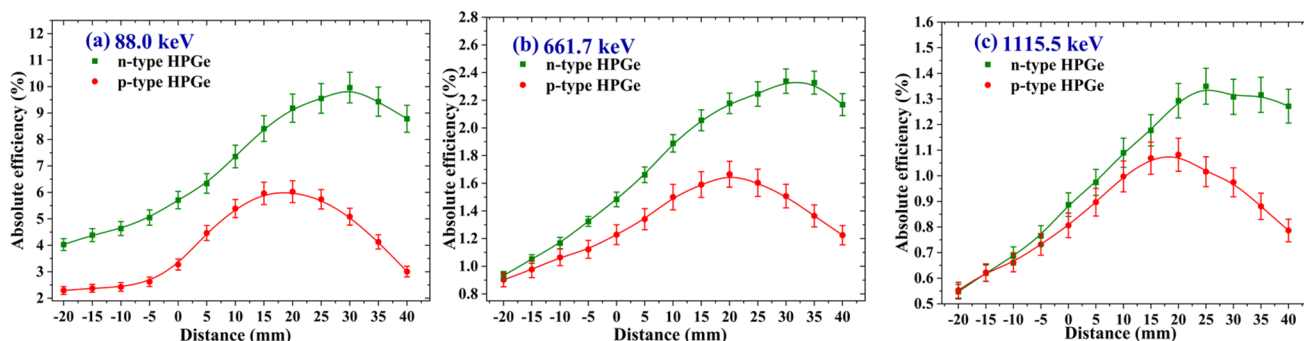

Fig. 9 Absolute photopeak efficiency at the energies of **a** 88.0 keV, **b** 661.7 keV and **c** 1115.5 keV, plotted against lateral scan within the uncertainty of source placement ≤ 1 mm

also evaluated and found maximum at 88.0 keV with the largest difference of 39.52% at 20 cm and 30 cm for p and n-type HPGe, respectively. At 661.7 keV maximum efficiency was found with a relative difference of 28.78%. On the characterization of both the detectors, the efficiency was measured at the energy of 1115.5 keV. The greatest absolute efficiency was evaluated at 20 and 25 mm in p and n-type HPGe, respectively, with a relative change of 19.82%.

Environmental background

The ambient background in the lab was monitored over more than 20 days using both detectors. In both cases, more than 90 background gamma lines were observed in day-wise spectra. Typical acquired background spectra employing both (p and n-type HPGe) detectors have been presented in Fig. 10, and the red curve corresponds to the acquired ambient background spectra in the p-type (GC-2018), while the blue curve corresponds to the acquired ambient background spectra in the n-type (GMX-20) HPGe. The difference between both the detectors is clearly visible in the spectra and shows that the overall registered ambient background in the n-type HPGe is above the background of p-type from 40 to 150 keV. Additionally, certain peaks such as 46.5 keV (^{210}Pb), 63.3 keV (^{234}Th) and, 129.1 keV (^{228}Ac) are visible above the background in n-type HPGe.

After 150 keV, the background is same but the peak height in the n-type detector is more than the p-type showing a bit higher active volume of n-type HPGe. The various natural radionuclides (^{238}U, ^{232}Th, their decay chain product, ^{40}K) as well as artificially influenced radionuclides (^{137}Cs and ^{60}Co) present in the background were identified in the spectra. The background analysis in both the detectors revealed that the highest activity (in cps) in the laboratory was found due to ^{40}K while the lowest was due to the ^{60}Co. The activity (in cps) of radionuclides is in the order of ^{40}K > ^{238}U > ^{232}Th > ^{137}Cs > ^{60}Co. To calculate the activity of ^{232}Th and ^{238}U, averages of the activity of their daughter radionuclides have been taken. ^{228}Ac in ^{232}Th and ^{214}Bi in ^{238}U were found most prominent radionuclides, emitting most gamma lines in the spectra. The greater contribution of all the radionuclides was registered in n-type HPGe, the reason is its higher sensitivity at low energy (< 150 keV) and higher energy due to a bit larger volume of the crystal than p-type. The energy, transition probability, and count rate (cps) of different gamma lines emitting from their respective radionuclides recorded in both detectors have been summarized in Table 5.

Further, the integral count rate has been calculated in various windows of a specific energy range for both the detectors and is shown in Table 6. The highest relative difference in count rate between both detectors was observed in the window from 40 to 150 keV which was 29.74%. Over the entire energy region of interest (40 to 2700 keV) for

Fig. 10 Three panel ambient background spectra observed (t = 86400 s) in p-type (in red) and n-type (in blue) HPGe with marked region from 40 keV to 150 keV. (Color figure online)
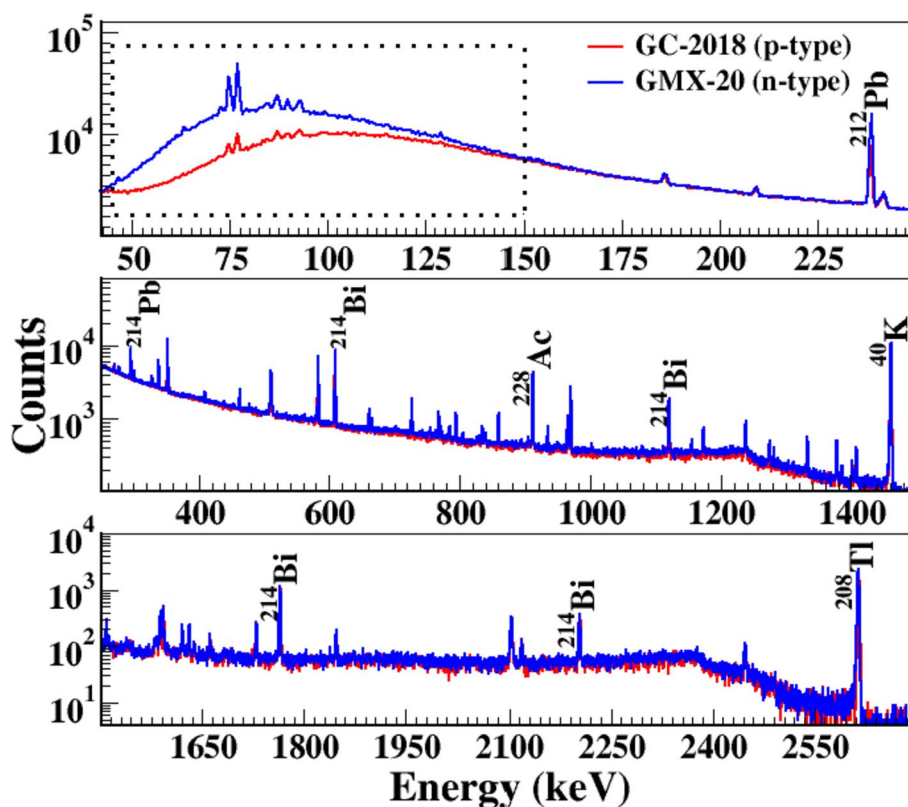
Table 5 Comparison of counts per second (cps) of major gamma photons emitted from their respective radionuclide sources present in the laboratory background and detected in p and n-type HPGe detectors

Source	Exact energy (keV)	Intensity (%)	cps (p-type) GC-2018	cps (n-type) GMX-20
(^{214}Pb, k$_{\alpha1}$)	77.1	9.70	0.077 ± 0.008	0.214 ± 0.010
^{228}Ac	129.1	2.42	0.018 ± 0.005	0.023 ± 0.005
^{212}Pb	238.6	43.60	0.316 ± 0.011	0.494 ± 0.009
^{214}Pb	295.2	18.42	0.143 ± 0.003	0.176 ± 0.003
Ann	510.8	22.60	0.122 ± 0.004	0.189 ± 0.008
^{214}Bi	609.3	45.49	0.251 ± 0.003	0.295 ± 0.003
^{137}Cs	661.7	85.10	0.013 ± 0.001	0.027 ± 0.002
^{228}Ac	911.2	25.80	0.121 ± 0.003	0.172 ± 0.003
^{214}Bi	1120.3	14.92	0.065 ± 0.002	0.075 ± 0.002
^{40}K	1460.8	10.66	0.432 ± 0.008	0.597 ± 0.010
^{214}Bi	1764.5	15.30	0.061 ± 0.002	0.070 ± 0.002
^{208}Tl	2614.5	99.75	0.128 ± 0.003	0.173 ± 0.004

Table 6 Comparison of background counts per second (cps) without shielding obtained for a specific integral window in p and n-type HPGe detector

Integral window (keV)	cps (p-type)	cps (n-type)	Relative difference (%)
40–150	43.79 ± 0.02	62.33 ± 0.03	29.74
150–500	38.73 ± 0.02	45.40 ± 0.02	14.70
150–1000	47.18 ± 0.02	55.84 ± 0.03	15.51
500–1000	8.45 ± 0.01	10.45 ± 0.01	19.12
1000–2000	4.48 ± 0.01	5.65 ± 0.01	20.69
40–2700	96.21 ± 0.03	124.81 ± 0.04	22.91

environmental radioactivity, the relative difference was found to be 22.91%.

Additionally, after acquiring ambient background in a separate laboratory using the n-type HPGe detector, the detector was shielded with lead (Pb) bricks, and data were subsequently collected. Figure 11 presents the ambient background measurements without shielding, with Pb-shielding, and the acquired soil sample spectra in a shielded configuration (with a measurement time of 86,400 s). These results are subsequently analyzed for various integral windows and presented in Table 7. Employing this setup, a reduction of 90.47% in background was achieved in the low-energy range (40–150 keV), and an 85.85% reduction in
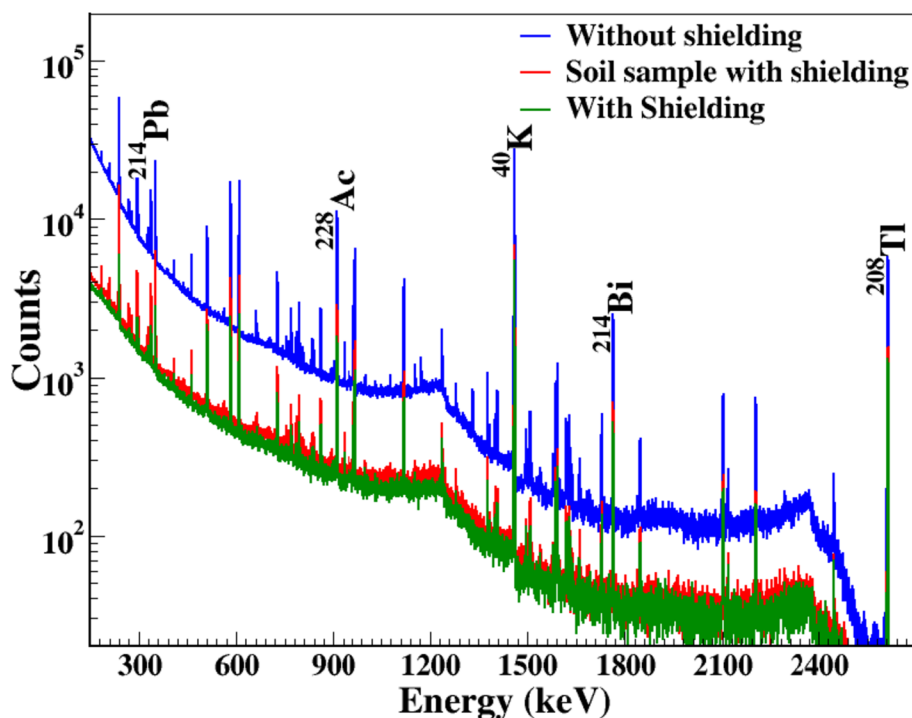

Fig. 11 Comparison of acquired ambient background without shielding, with Pb-shielding, and soil sample spectra with shielding (t = 86400 s) in n-type HPGe detector

Table 7 Comparison of integral count rates in different configurations with various energy windows using n-type HPGe. The background data in Table were obtained in a laboratory that is different from the one depicted in Table 6

Integral window (keV)	Without shielding (cps) A	With shielding (cps) B	Soil sample with shielding (cps)	$((B - A)/A) \times 100$
40–150	104.84 ± 0.03	9.99 ± 0.01	13.25 ± 0.01	90.47
150–1000	111.69 ± 0.04	19.32 ± 0.01	22.61 ± 0.02	82.70
1000–2000	11.68 ± 0.01	2.76 ± 0.01	3.27 ± 0.01	76.40
40–2700	230.26 ± 0.05	32.57 ± 0.02	39.72 ± 0.02	85.85

background was observed within the mean energy region of interest (40–2700 keV) for environmental radioactivity. It is necessary to mention here that the data of the spectra shown in Fig. 10 were acquired in one laboratory for both detectors, while the data of the spectra displayed in Fig. 11 were obtained from another laboratory.

Summary and conclusions

This work initiated with the optimization and systematic calibration of n and p-type HPGe detectors and further, we studied their essential parameters such as resolution, efficiency, MDA, FoM, and peak shape, etc. These characteristics were studied in the wide energy range of 40–1408 keV with various source-detector configurations. The overall MDA values in both detectors for energies greater than 150 keV either remain close to unity or are less than unity (~ 1 Bq). The orientation of crystals with their active volumes was studied by performing the detail characterization with close scanning (distance, lateral, and radial) and evaluating the counting efficiency in close geometry. The scanning was conducted utilizing standard gamma sources without a collimator. Intercomparison between the performance of n and p-type HPGe detectors on the basis of efficiency and background spectral analysis was carried out. The n-type HPGe detector is more suitable for the lower energy (≤ 150 keV) region for gamma spectroscopy, however, in the high energy region both (p and n-type HPGe) performed the same. The n-type HPGe's high efficiency at low energies can also be attributed to the presence of its thin beryllium (Be) window. It is important to explore and quantify the background surrounding the setup prior to measuring the radioactivity of the environmental sample as it consists the low-level radioactivity. Hence, acquired background spectra in both detectors were compared. The relative ratio in integral count rate between both the detectors in the energy range from 40 keV to 150 keV was found to be 29.74%. The contribution of ^{232}Th was observed to be slightly higher than ^{238}U, while the radioactivity of ^{40}K was the highest, which may be attributed to laboratory flooring. Employing n-type HPGe in a Pb-shielded configuration has led to a significant reduction of 85.85% in the overall background within the energy range of 40–2700 keV. Characterization and performance of n and p-type HPGe detectors show that both the detectors are in good working condition and can be used for the investigation of environmental radioactivity study. Dual layer Pb-shielding to suppress gamma contributions and an inner copper layer to eliminate X-rays from the background are future tasks to make it more compact.

Declaration

Conflict of interest The authors declare that they have no known conflict of interest.

References

1. Eberth J, Simpson J (2008) From Ge (Li) detectors to gamma-ray tracking arrays–50 years of gamma spectroscopy with germanium detectors. Prog Part Nucl Phys 60(2):283–337. https://doi.org/10.1016/j.ppnp.2007.09.001
2. Knoll GF (2010) Radiation detection and measurement, 4th edn. Wiley
3. Islam MN, Akhter H, Begum M, Mawla Y, Kamal M (2018) Study of a laboratory-based gamma spectrometry for food and environmental samples. Intern J Adv Eng, Manag Sci. 4(1):239956. https://doi.org/10.22161/ijaems.4.1.5
4. Trang LTN, Chuong HD, Thanh TT (2021) Optimization of p-type HPGe detector model using Monte Carlo simulation. J Radioanal Nucl Chem 327(1):287–297. https://doi.org/10.1007/s10967-020-07473-2
5. Vargas MJ, Timón AF, Díaz NC, Sánchez DP (2002) Influence of the geometrical characteristics of an HpGe detector on its efficiency. J Radioanal Nucl Chem 253(3):439–443. https://doi.org/10.1023/A:1020425704745
6. Spieler H (2005) Semiconductor detector systems. Vol 12. Oxford university press
7. Boson J, Ågren G, Johansson L (2008) A detailed investigation of HPGe detector response for improved Monte Carlo efficiency calculations. Nucl Instrum Methods Phys Res, Sect A 587(2–3):304–314. https://doi.org/10.1016/j.nima.2008.01.062

8. Zamzamian SM, Hosseini SA, Samadfam M (2017) Optimization of the marinelli beaker dimensions using genetic algorithm. J Environ Radioact 172:81–88. https://doi.org/10.1016/j.jenvrad.2017.03.020

9. Gilmore G (2008) Practical Gamma-ray Spectrometry, 2nd edition. Wiley, ISBN: 978–0–470–86196–7

10. Done L, Ioan MR (2016) Minimum detectable activity in gamma spectrometry and its use in low level activity measurements. Appl Radiat Isot 114:28–32. https://doi.org/10.1016/j.apradiso.2016.05.004

11. Mei-Woo Y (2014) Determination performance of gamma spectrometry co-axial HPGE detector in radiochemistry and environment group. Nuclear Malaysia 46(1):1–7

12. Usman A, Nor NM (2019) Test performance of gamma spectrometry co-axial high purity germanium detectors in universiti teknologi malaysia. IOSR J Appl Phys 11(6):58–66. https://doi.org/10.9790/4861-1106015866

13. Dragounová L, Rulík P (2013) Low level activity determination by means of gamma spectrometry with respect to the natural background fluctuation. Appl Radiat Isot 81:123–127. https://doi.org/10.1016/j.apradiso.2013.03.017

14. Yadav M, Prasad M, Joshi V, Gusain GS, Ramola RC (2016) A comparative study of radium content and radon exhalation rate from soil samples using active and passive techniques. Radiat Prot Dosimetry 171(2):254–256. https://doi.org/10.1093/rpd/ncw069

15. Mesrar H, Sadiki A, Faleh A, Quijano L, Gaspar L, Navas A (2017) Vertical and lateral distribution of fallout 137Cs and soil properties along representative toposequences of central Rif, Morocco. J Environ Radioact 169:27–39. https://doi.org/10.1016/j.jenvrad.2016.12.012

16. Kandari T, Prasad M, Pant P, Semwal P, Bourai AA, Ramola RC (2018) Study of radon flux and natural radionuclides (226Ra, 232Th and 40K) in the main boundary thrust region of Garhwal Himalaya. Acta Geophys 66:1243–1248. https://doi.org/10.1007/s11600-018-0158-6

17. Prasad M, Ranga V, Kumar GA, Ramola RC (2020) Radiological impact assessment of soil and groundwater of Himalayan regions in Uttarakhand, India. J Radioanal Nucl Chem 323:1269–1282. https://doi.org/10.1007/s10967-019-06827-9

18. Kumar A, Singh P, Semwal P, Singh K, Prasad M, Ramola RC (2021) Study of primordial radionuclides and radon/thoron exhalation rates in Bageshwar region of Kumaun Himalaya, India. J Radioanal Nucl Chem 328:1361–1367. https://doi.org/10.1007/s10967-020-07582-y

19. Joel ES, Maxwell O, Adewoyin OO, Olawole OC, Arijaje TE, Embong Z, Saeed MA (2019) Investigation of natural environmental radioactivity concentration in soil of coastaline area of Ado-Odo/Ota Nigeria and its radiological implications. Sci Rep 9(1):4219. https://doi.org/10.1038/s41598-019-40884-0

20. UNSCEAR (1982) United nations scientific committee on the effects of atomic radiation. Exposures resulting from nuclear explosions

21. Inoue K, Fukushi M, Van Le T, Tsuruoka H, Kasahara S, Nimelan V (2020) Distribution of gamma radiation dose rate related with natural radionuclides in all of Vietnam and radiological risk assessment of the built-up environment. Sci Rep 10(1):12428. https://doi.org/10.1038/s41598-020-69003-0

22. Wallbrink PJ, Walling DE, He Q (2003) Radionuclide measurement using HPGe gamma spectrometry. In: handbook for the assessment of soil erosion and sedimentation using environmental radionuclides. 67–96 Springer. https://doi.org/10.1007/0-306-48054-9_5

23. Ramadhan RA, Abdullah KM (2018) Background reduction by Cu/Pb shielding and efficiency study of NaI (TI) detector. Nucl Eng Technol 50(3):462–469. https://doi.org/10.1016/j.net.2017.12.016

24. Linux advanced multi parameter system. URL: https://www.tifr.res.in/~pell/lamps.html

25. Thakur S, Devi S, Kaintura SS, Tiwari K, Singh PP (2023) Spectroscopic performance evaluation and modeling of a low background HPGe detector using GEANT4. Nucl Instrum Methods Phys Res, Sect A 1058:168826. https://doi.org/10.1016/j.nima.2023.168826

26. Tsoulfanidis N, Landsberger S (2021) Measurement and detection of radiation. 5th edn. CRC press. https://doi.org/10.1201/9781003009849

27. Keyser RM, Twomey TR (2013) Optimization of pulse processing parameters for HPGe gamma-ray spectroscopy systems used in extreme count rate conditions and wide count rate ranges. J Radioanal Nucl Chem 296(1):503–508. https://doi.org/10.1007/s10967-012-2113-3

28. Fairstein E, Wagner S (1997) IEEE standard test procedures for germanium gamma-ray detectors. IEEE Std. https://doi.org/10.1109/IEEESTD.1997.82400

29. Currie LA (1968) Limits for qualitative detection and quantitative determination. Appl radiochem Anal chem 40(3):586–593. https://doi.org/10.1021/ac60259a007

30. Abbas MI (2006) HPGe detector absolute full-energy peak efficiency calibration including coincidence correction for circular disc sources. J Phys D Appl Phys 39(18):3952. https://doi.org/10.1088/0022-3727/39/18/005

31. Demir D, Eroğlu M, Turşucu A (2013) Studying of characteristics of the HPGe detector for radioactivity measurements. J Instrum 8(10):P10027. https://doi.org/10.1088/1748-0221/8/10/P10027